C3S Greenhouse Gas (GHG: MTCO2 v10.1 & MTCH4 v10.2): Algorithm Theoretical Basis Document (ATBD)

Last modified on Sept. 10, 2025 08:45

Contributors: C. Crevoisier (Laboratoire de Météorologie Dynamique (LMD)/CNRS), N. Meilhac (FX-CONSEIL/Laboratoire de Météorologie Dynamique (LMD))

Issued by: Laboratoire de Météorologie Dynamique/CNRS, France

Date: 19.10.2024

Ref: C3S2_313a_DLR_WP1-DDP-GHG-v1_ATBD_MTCO2_v10.1_MTCH4_v10.2

Official reference number service contract: 2024/C3S2_313a_DLR/SC1

Table of Contents

History of modifications

› Click here to expand the list of modifications

Product Version	Issue	Date	Description of modification	Chapters / Sections
MTCO2 v10.1, MTCH4 v10.2	1	19-November-2024	New document	All
MTCO2 v10.1, MTCH4 v10.2	2	12-May-2025	Updated following revision of independent reviewers	All
MTCO2 v10.1, MTCH4 v10.2	3	28-August-2025	Minor adjustments after independent review and finalisation for publication	All

List of datasets covered by this document

› Click here to expand the list of datasets covered by this document

Deliverable ID	Product title	Product type (CDR, ICDR)	Version number	Delivery date
WP1-DDP-GHG-v1	MTCO2_OBS4MIPS	CDR	10.1	31-Oct-2024
WP1-DDP-GHG-v1	MTCH4_OBS4MIPS	CDR	10.2	31-Oct-2024

Acronyms

› Click here to expand the list of acronyms

Acronym	Definition
AMSU-A	Advanced Microwave Sounding Unit A

ATBD	Algorithm Theoretical Basis Document
C3S	Copernicus Climate Change Service
CCI	Climate Change Initiative
CDR	Climate Data Record
CDS	(Copernicus) Climate Data Store
CMUG	Climate Modelling User Group (of ESA's CCI)
ECMWF	European Centre for Medium Range Weather Forecasting
ECV	Essential Climate Variable
EOS	Earth Observing System
ESA	European Space Agency
EU	European Union
EUMETSAT	European Organisation for the Exploitation of Meteorological Satellites
FCDR	Fundamental Climate Data Record
GHG	GreenHouse Gas
IASI	Infrared Atmospheric Sounding Interferometer
L1	Level 1
L2	Level 2
L3	Level 3
LMD	Laboratoire de Météorologie Dynamique
MT	Mid-tropospheric
NASA	National Aeronautics and Space Administration
NetCDF	Network Common Data Format
NLIS	LMD/CNRS *neuronal* network mid/upper tropospheric CO2 and CH4 retrieval algorithm
NOAA	National Oceanic and Atmospheric Administration
Obs4MIPs	Observations for Climate Model Intercomparisons
ppb	Parts per billion
ppm	Parts per million
PQAR	Product Quality Assessment Report
RTM	Radiative transfer model
TIR	Thermal Infra Red
TR	Target Requirements
TRD	Target Requirements Document
URD	User Requirements Document

General definitions

Essential climate variable (ECV): An ECV is a physical, chemical, or biological variable or a group of linked variables that critically contributes to the characterization of Earth's climate (Bojinski et al., 2014).

Climate data record (CDR): The US National Research Council (NRC) defines a CDR as a time series of measurements of sufficient length, consistency, and continuity to determine climate variability and change (National Research Council, 2004).

Fundamental climate data record (FCDR): A fundamental climate data record (FCDR) is a CDR of calibrated and quality-controlled data designed to allow the generation of homogeneous products that are accurate and stable enough for climate monitoring.

Thematic climate data record (TCDR): A thematic climate data record (TCDR) is a long time series of an essential climate variable (ECV) (Werscheck, 2015).

Intermediate climate data record (ICDR): An intermediate climate data record (ICDR) is a TCDR which undergoes regular and consistent updates (Werscheck, 2015), for example because it is being generated by a satellite sensor in operation.

Satellite data processing levels: The NASA Earth Observing System (EOS) distinguishes six processing levels of satellite data, ranging from Level 0 (L0) to Level 4 (L4) as follows (Parkinson et al., 2006).

L0	Unprocessed instrument data
L1A	Unprocessed instrument data alongside ancillary information
L1B	Data processed to sensor units (geo-located calibrated spectral radiance and solar irradiance)
L2	Derived geophysical variables (e.g., XCO_2) over one orbit

L3	Geophysical variables averaged in time and mapped on a global longitude/latitude horizontal grid
L4	Model output derived by assimilation of observations, or variables derived from multiple measurements (or both)

Absolute systematic error or systematic error: Component of measurement error that in replicate measurements remains constant or varies in a predictable manner. Note that "systematic error" refers to the absolute systematic error (in contrast to "relative systematic error" defined below). For satellite GHG ECV products especially the relative systematic error is important.

Relative systematic error, relative accuracy or relative bias: Identical with "Systematic error" but after bias correction and without considering a possible global offset (overall mean bias). Reflects the importance of spatially and temporally correlated errors (spatio-temporal biases). Computed from standard deviations of spatial and temporal biases.

Bias: Estimate of a systematic measurement error.

Precision: Measure of reproducibility or repeatability of the measurement without reference to an international standard so that precision is a measure of the random and not the systematic error. Suitable averaging of the random error can improve the precision of the measurement but does not establish the systematic error of the observation (CMUG-RBD, 2012).
Note: Precision is quantified with the standard deviation (1-sigma) of the error distribution.

Stability: Term often invoked with respect to long-term records when no absolute standard is available to quantitatively establish the systematic error - the bias defining the time-dependent (or instrument-dependent) difference between the observed quantity and the true value (CMUG-RBD, 2012).
Note: Stability requirements cover inter-annual error changes. If the change in the average bias from one year to another is larger than the defined values, the corresponding product does not meet the stability requirement.

Representativity: Extent to which an average of a set of measured values corresponds to the true average, e.g., over a grid cell. It is important when comparing with or assimilating in models. Measurements are typically averaged over different horizontal and vertical scales compared to model fields. If the measurements are smaller scale than the model it is important. The sampling strategy can also affect this term (CMUG-RBD, 2012).

Threshold requirement: The threshold is the limit at which the observation becomes ineffectual and is not of use for climate-related applications (CMUG-RBD, 2012).

Goal requirement: The goal is an ideal requirement above which further improvements are not necessary (CMUG-RBD, 2012).

Breakthrough requirement: The breakthrough is an intermediate level between the "threshold" and "goal" requirements, which - if achieved - would result in a significant improvement for the targeted application. The breakthrough level may be considered as an optimum, from a cost-benefit point of view when planning or designing observing systems (CMUG-RBD, 2012).

Horizontal resolution: Area over which one value of the variable is representative of (CMUG-RBD, 2012).

Vertical resolution: Height over which one value of the variable is representative of. Only used for profile data (CMUG-RBD, 2012).

Observing Cycle (or **Revisit Time**): Temporal frequency at which the measurements are required (CMUG-RBD, 2012).

Averaging kernel: Vertical sensitivity of the retrieval to greenhouse gas mixing ratios.

NLIS: Non Linear Inference Scheme is the retrieval code based on artificial neural networks designed by LMD to infer mid-tropospheric columns of CO_2 and CH_4 from coupled infrared and microwave observations.

Executive summary

This document is an Algorithm Theoretical Basis Document (ATBD) generated in the framework of the Copernicus Climate Change Service (C3S, https://climate.copernicus.eu/). For C3S a large number of satellite-derived Essential Climate Variable (ECV) data products are generated and made available via the Copernicus Climate Data Store (CDS, https://cds.climate.copernicus.eu/).

This document describes how two satellite-derived atmospheric mid-tropospheric column of carbon dioxide (MT-CO_2) and methane (MT-CH_4) Level 3 products have been generated. This document describes the retrieval algorithms (CNRS-LMD *Non Linear Inference Scheme* -NLIS) to generate the Level 2 (L2) products from the three platforms Metop-A, -B and -C and how these L2 products are merged to obtain the Level 3 (L3) MTCO2_OBS4MIPS and MTCH4_OBS4MIPS products.

MT-CO_2 and MT-CH_4 products are mid-tropospheric-averaged air mixing ratios (mole fractions) of CO_2 and CH_4 products (noted as MT-CO_2 and MT-CH_4) derived from observations made by simultaneous observations of the IASI and AMSU-A instruments flying together onboard the three successive Metop-A (July 2007-August 2021), -B (since February 2013) and -C (since May 2019) satellites using a non-linear inference scheme (NLIS) using Multi-Layer Perceptrons. IASI hyperspectral observations in the thermal infrared at 7.7 µm for CH_4 and at 15 µm for CO_2, which are sensitive to both temperature and gas concentrations of CH_4/CO_2 are used in conjunction with microwave observations form the AMSU-A instruments, only sensitive to temperature, to decorrelate temperature variations from CO_2/CH_4 variations in the infrared radiance (Crevoisier et al., 2009a, 2009b, 2013). Retrievals are thus performed at the AMSU-A field-of-view resolution which is 40km at nadir, for a swath of 2200 km, with a spatial coverage of about 60°S to 60°N for MT-CH_4 and about 30°S to 30°N for MT-CO_2, twice a day at 9:30 am/pm local time.

It should be noted that the IASI instrument onboard Metop-B is still operational. However, the degradation of the AMSU-A instrument, more precisely tropospheric channel 6, onboard Metop-B has significantly degraded the quality of MT-CH_4 retrievals after December 2021. Therefore, L2 MT-CH_4 products from Metop-B are no longer provided from December 2021.

The MTCO2_OBS4MIPS and MTCH4_OBS4MIPS products are merged multi-sensor MT-CO_2 and MT-CH_4 L3 products with daily time and 1^ox1^o spatial resolution generated using an ensemble of individual satellite sensor L2 MT-CO_2 and MT-CH_4 products from Metop-A, -B and -C available between July 2007 and December 2023 (updated every 6 months).

Direct link to CO_2 products: https://cds.climate.copernicus.eu/datasets/satellite-carbon-dioxide?tab=overview, DOI: 10.24381/cds.f74805c8

Direct link to CH_4 products: https://cds.climate.copernicus.eu/datasets/satellite-methane?tab=overview, DOI: 10.24381/cds.b25419f8

This document describes the instruments used to obtain the L2 MT-CO_2 and MT-CH_4 in Section 1, the input data used to calculate MT-CO_2 and MT-CH_4 in Section 2, the algorithm used to generate the L2 and L3 products in Section 3 and the MTCO2_OBS4MIPS and MTCH4_OBS4MIPS products in Section 4.

1. Missions and Instruments

1.1. The IASI instrument onboard the Metop satellites

The Infrared Atmospheric Sounding Interferometer (IASI) is a high resolution Fourier Transform Spectrometer based on a Michelson Interferometer coupled to an integrated imaging system that measures infrared radiation emitted from the Earth (https://iasi.cnes.fr/en/IASI/index.htm). Developed by the Center National d'Etudes Spatiales (CNES) in collaboration with the European Organisation for the Exploitation of Meteorological Satellites (EUMETSAT), IASI was launched in October 2006 onboard the polar orbiting Meteorological Operational Platform (Metop-A), in September 2012 onboard Metop-B, and in October 2018 onboard Metop-C. Metop-A has been decommissioned in November 2022, after 15 years of nominal operation. The last data delivery happened on October 15th 2022. Starting in late August 2021, so-called end-of-life experiments were conducted by CNES and EUMETSAT, yielding a few days without data, as well as a full month (September 15th to October 15th 2022) with IASI operating in a narrow swath configuration (220 km instead of 2200 km) in order to provide oversampling along the orbits.

The comparison between the 3 IASI instruments at Level 1 shows that the three instruments agree at the level of 0.1 K, in term of brightness temperature, or less for most of the spectrum.

IASI provides 8461 spectral samples, ranging from 645 cm^{-1} to 2760 cm^{-1} (15.5 µm and 3.6 µm), with a spectral sampling interval of 0.25 cm^{-1}, and a spectral resolution of 0.5 cm^{-1} (see Technical Specification in Table 1 for more details). IASI is an across track scanning system, whose swath width is of 2200 km, allowing global coverage twice a day. As seen in Figure 1, the instantaneous Field of View (IFOV) is sampled by 2×2 circular pixels whose ground resolution is 12 km at nadir at 9:30 am/pm local time.

The combined use of two successive Metop satellites, which are flying on the same orbit but with nearly half an orbit out of phase, yields a complete coverage of the Earth in one day. Combining Metop-A, -B and -C, the time series will cover about 20 years. In order to be useful for climate studies, it is mandatory that the time series derived from the 3 successive platforms are consistent in order to allow the study of trends and growth rates of several essential climate variables such as greenhouse gases.

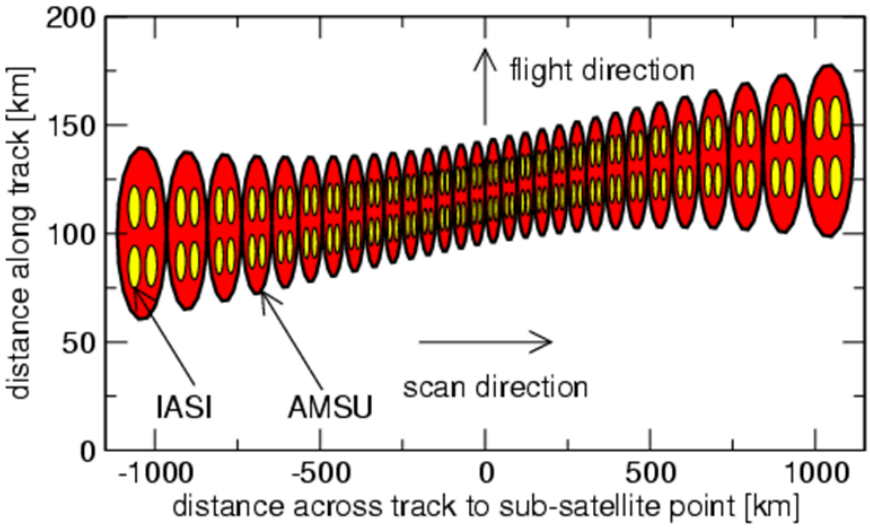

Figure 1: IASI and AMSU-A scanning geometry. IASI individual field of views are shown as yellow circles while AMSU-A individual field of views are shown as red circles (from IASI Level 1 Product Guide available at http://eodg.atm.ox.ac.uk/user/dudhia/iasi/documents/PDF_IASI_LEVEL_1_PROD_GUIDE.pdf).

1.2. The AMSU-A instrument onboard the Metop satellites

Also flying onboard Metop satellites is the AMSU-A (Advanced Microwave Sounding Unit) instrument, which is a 15-channel microwave radiometer, measuring scene radiances in 15 discrete frequency channels spanning 23-90 GHz. Thirty consecutive field of views of 48 km diameter at nadir are sampled, yielding a 2,074 km swath width. AMSU-A uses oxygen absorption bands/lines for atmospheric temperature sounding, while window channels provide information on surface temperature and emissivity.

As seen in Figure 1, scanning of both sounders is synchronized, with 4 IASI fields of view (FOV) (yellow lozenges) embedded in 1 AMSU-A FOV (red lozenge), allowing the same atmospheric situation to be simultaneously observed by both instruments.

On all Metop satellites, several AMSU-A channels have experienced behaviors outside of specifications. In particular, among the 3 AMSU-A channels 6, 7 and 8 that are particularly important for the retrieval procedure, only the AMSU-A channel 6 stays available for all Metop satellites for the whole time period covered by each satellite. For instance, for Metop-A, the AMSU-A channel 7 stopped operating in 2008 while AMSU-A channel 8 stopped operating in 2015. This has led to some changes in the retrieval procedure that are described below.

2. Input and auxiliary data

2.1. Level 1 data

IASI and AMSU-A input data are Level 1c and Level 1b radiance data respectively, disseminated in near-real time through the EUMETCast system of EUMETSAT. Metop-A data have been available between July 2007 and September 2021 when Metop-A was decommissioned. AMSU-A input data onboard Metop-B data have been available between February 2013 and December 2021. IASI data onboard Metop-B have been available since February 2013. IASI and AMSU-A data onboard Metop-C are available since July 2019. These Level 1 data are used to calculate L2 MT-CO_2 and MT-CH_4 products using the L2 IASI algorithm (see Section 3.1). The following tables provide an overview of the characteristics of IASI (Table 1) and AMSU-A (Table 2) respectively.

Table 1: Overview of IASI characteristics.

Originating System	Infrared Atmospheric Sounding Interferometer (IASI) onboard the three successive platform Metop-A, B & C
Data class	Earth observation
Key technical characteristics	• Fourier transform spectrometer • 8461 spectral samples, ranging from 645 cm^{-1} to 2760 cm^{-1} (15.5 µm and 3.6 µm) with a spectral sampling of 0.25 cm^{-1}, and a spectral resolution of 0.5 cm^{-1} • Across track scanning system: a scan range of 48°20′ on either side of the nadir direction (around 2×1100 km) • 30 (15 in each 48°20′ branch) measurements positions that each contain 2X2 IASI IFOV • 8 seconds to acquire data from one complete across track (around 1 300 000 spectra per day)
Data Availability and Coverage	Coverage: 180°W 90°S – 180°E 90°N Metop-A: July 2007 - September 2021 (decommissioned) Metop-B: February 2013 - today Metop-C: July 2019 - today
Source Data Name and Product Technical Specifications	IASI Level 1c Technical Specification: https://user.eumetsat.int/s3/eup-strapi-media/pdf_iasi_pg_487c765315.pdf
Data Quality and Reliability	Validation reports: https://user.eumetsat.int/s3/eup-strapi-media/pdf_iasi_level1_day2_rpt_v2_dbd49e55ea.pdf

Ordering and delivery mechanism	EUMETCast system (EUMETSAT): https://user.eumetsat.int/data-access/eumetcast-europe

Table 2: Overview of AMSU-A characteristics.

Originating System	Advanced Microwave Sounding Unit A (AMSU-A) onboard the three successive platform Metop-A, B & C
Data class	Earth observation
Key technical characteristics	• Microwave sounders; • AMSU-A measures in 15 spectral bands: two channels at 23.8 GHz and 31.4 GHz and twelve channels in the range 50.3 GHz up to 57.290344 GHz plus one channel at 89.0 GHz; • Across track scanning system: a scan range of f ± 48.33° with respect to the nadir direction (around 2×1100 km); • 30 (15 in each 48°20′ branch) measurements positions; • 8 seconds to acquire data from one complete across track;
Data Availability and Coverage	Coverage: 180°W 90°S – 180°E 90°N Metop-A: July 2007 - September 2021 (decommissioned) Metop-B: February 2013 – today (since end of 2021: AMSU-A channel 6 is unusable) Metop-C: July 2019 – today
Source Data Name and Product Technical Specifications	AMSU-A Level 1b Technical Specification: https://user.eumetsat.int/s3/eup-strapi-media/pdf_ten_990005_eps_amsal1_pgs_6ccda24e33.pdf
Data Quality and Reliability	Long-Term Monitoring: https://www.star.nesdis.noaa.gov/icvs/
Ordering and delivery mechanism	EUMETCast system (EUMETSAT): https://user.eumetsat.int/data-access/eumetcast-europe

2.2. Other data

2.2.1. The TIGR database

The CNRS-LMD Non Linear Inference Scheme (NLIS) used to retrieve mid-tropospheric columns of greenhouse gases is based on artificial neural networks trained on a dataset of well-known atmospheric situations: the Thermodynamic Initial Guess Retrieval (TIGR, Chevallier et al., 1998). In its latest version, available at https://ara.lmd.polytechnique.fr/index.php?page=tigr (last access: 09-06-2024), it is a climatological library of 2311 representative atmospheric situations selected by statistical methods from 80,000 radiosonde reports. Each situation is described, from the surface to the top of the atmosphere, by the values of the temperature, water vapour and ozone concentrations on a given pressure grid. For each situation are available the radiances of each IASI/AMSU-A channel simulated under several conditions of observation (satellite zenith angle, surface characteristics, etc.), as well as the atmospheric transmittances and Jacobians (partial derivatives of the brightness temperature with respect to temperature, gas concentration for H_2O, O_3, CO_2, N_2O CO, CH_4, surface temperature and emissivity). For CO_2, mixing ratios range is from 345 to 445 ppm; for CH_4, mixing ratios range is from 1610 ppb to 2110 ppb. Radiances, transmittances and Jacobians profiles are generated using the 4A/OP forward radiative transfer model (Scott and Chédin, 1981).

2.2.2. The ARSA database

The computation of the radiative biases, which plays a critical role in the retrieval process, is based on the ARSA (Analyzed RadioSoundings Archive) database, which is available at http://ara.abct.lmd.polytechnique.fr/index.php?page=arsa (last access: 01-03-2025). ARSA builds on radiosonde observations made by worldwide distributed radiosonde stations and combines them with surface and other auxiliary observations. Physically coherent quality control tests have been developed to detect and eliminate gross errors: format problems, redundant radiosounding and levels, unrealistic jumps, physically implausible values, temporal and vertical inconsistencies in temperature and dew point temperatures. The current ARSA database (about 6 million elements) starts in January 1979, and is extended onwards, on a monthly basis.

3. Algorithms

3.1. Algorithm for L2 IASI mid-tropospheric CO_2 and CH_4 retrieval

3.1.1. General description

Mid-tropospheric columns of methane (CH_4) and carbon dioxide (CO_2) are retrieved from simultaneous observations of the IASI and AMSU instruments flying together onboard the Metop satellites using a non-linear inference scheme. As described in Crevoisier et al. (2009a,b), this scheme is based on artificial neural networks called Multilayer Perceptron (MLP) neural network (Rumelhart et al., 1986) with two hidden layers. Choosing such an approach stems from the weakness of the signal induced on IASI radiances by CO_2 and CH_4 variations, associated with the complexity (in particular its non-Gaussian behavior and the low signal-to-noise ratio) of the relationship between CO_2 or CH_4 concentration and observed radiances, which makes it difficult to retrieve the mid-tropospheric CO_2 and CH_4 column from infrared radiances with the precision needed for scientific studies. Introduced to derive tropospheric CO_2 integrated content from TOVS (Chédin et al., 2003), NLIS has been modified to process observations from IASI.

The main difficulty in estimating global distribution of CO_2 or CH_4 from infrared sounders comes from the fact that infrared measurements are sensitive, to the first order, to both temperature and CO_2/CH_4 variations (the IASI channels selected to retrieve MT-CO_2/CH_4 columns have reduced sensitivity to H_2O). Independent information on temperature is thus needed to allow the separation of these two effects. IASI hyperspectral observations in the thermal infrared, which are sensitive to both temperature and gas concentrations of CO_2 or CH_4, are used in conjunction with microwave observations from the AMSU-A instruments, which are only sensitive to temperature, to decorrelate both signals. For CH_4, IASI channels located in the 7.7 µm spectral region are used; for CO_2, channels located in the 15 µm region are used.

Only a subset of channels presenting the best properties with regards to the retrieval performances, for instance in terms of gas sensitivity and vertical coverage as explained in Crevoisier (2018), are used. The neural networks are trained on a learning dataset with couples of known inputs-outputs coming from the TIGR database and then are evaluated on an evaluation dataset (the ARSA database). The retrievals are performed during day and night-time (9:30 am/pm local time), both over land and over sea. The CO_2 retrievals are limited to the tropical airmasses (about 30°N to 30°S); this is because the decorrelation between CO_2 and temperature signals in the IASI radiances is more complex outside of the tropical band due to the higher variability of the temperature profile compared to the tropical one, yielding too high retrieval uncertainty.

Through comparisons with regular aircraft (Machida et al., 2008) or balloon (Membrive et al., 2017) measurements as well as observations made at the surface, we have shown (e.g. Crevoisier et al., 2013) that, once the radiometric characterization of the instruments is performed, IASI and AMSU-A capture well the trend and interannual variation of CO_2/CH_4 giving confidence in the ability of IASI and AMSU-A to follow its evolution over the 20 years of the Metop program.

Figure 2 shows a flow diagram of the preparation of the learning database and the training of the Multi-Layer Perceptrons (MLPs), and application to IASI/AMSU-A observations:

- The training database is computed using TIGR and GEISA (Gestion et Etude des Informations Spectroscopiques Atmosphériques, Jacquinet-Husson et al., 2011) and the 4A/OP radiative code;
- This training database is used for the training of MLPs.
- "Clear sky" IASI/AMSU-A observations in terms of brightness temperature are presented to MLPs to obtain the MT-CO_2/CH_4 retrievals;

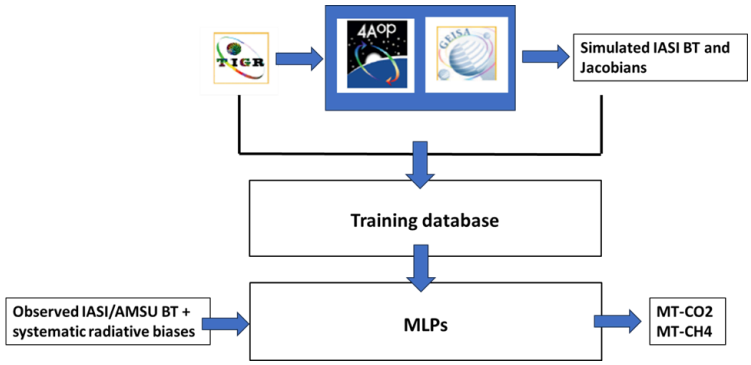

Figure 2: Flow diagram of the preparation of the learning database and the training of Multilayer Perceptrons (MLPs), and application to IASI/AMSU-A brightness temperatures (BT).

The availability of L2 MT-CO_2 and MT-CH_4 products for the three Metop-A, -B and -C platforms between July 2007 and December 2023 is illustrated in Figure 3.

For Metop-A, the MT-CO_2 and MT-CH_4 products are available between 2007/07/01 and 2021/08/31; for Metop-B, between 2013/02/01 and 2021/12/31 (before the products are impacted by the degradation of the AMSU-A noise); for Metop-C, between 2019/05/01 and 2023/12/31.

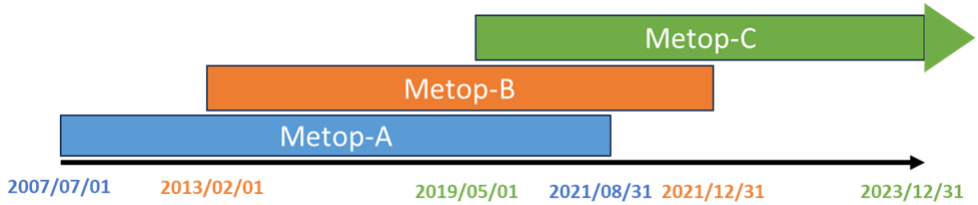

Figure 3: This diagram illustrates the availability of L2 MT-CO_2 and MT-CH_4 products for the three Metop-A, -B and -C platforms between July 2007 and December 2023

3.1.2. Forward model and spectroscopic database

The radiative simulations in the thermal infrared range performed in this study are based on the fast and accurate line-by-line radiative transfer model 4A (Automatized Atmospheric Absorption Atlas) (Scott and Chédin, 1981). the 4A model is an advanced version of the nominal line-by-line STRANSAC model (Scott, 1974) and is basically a compressed look-up-table of optical depths calculated once and for all. It can be coupled to any spectroscopic databases and can simulate any instrumental configurations (ground, airborne, satellite). In addition to the simulation of atmospheric transmissions and radiance (or equivalently brightness temperature (BT)) spectra, 4A model analytically computes Jacobians for all relevant atmospheric variables. Jacobians are defined as the partial derivative of the channel brightness temperature with respect to a layer physical variable such as a gas mixing ratio, a temperature or the emissivity. Since the beginning of 2001, an operational version of 4A denoted as 4A/OP has been developed by the company Noveltis (https://4aop.noveltis.com/, last access: 16/03/2025) in collaboration with CNES and LMD. The 4A/OP model is the official code chosen by CNES for calibration/validation and preparation activities of several space missions, including IASI and IASI-NG. For this study, the spectrometric parameters used as inputs to 4A/OP, are taken from the GEISA-2011 database (Jacquinet-Husson et al., 2011).

3.1.3. Channel selection

IASI presents 8461 channels covering most of the infrared spectrum. Approximately a hundred of them are sensitive to CH_4, whilst a few hundred are sensitive to CO_2.

3.1.3.1. Channels for CH_4

IASI channels sensitive to CH_4 are either located in band v_4 of CH_4, around 7.7 µm (1306 cm^{-1}), or in band v_3, around 3.8 µm (2630 cm^{-1}). The sensitivity to CH_4 concentration variations of channels located in the 3.8 µm band is much lower than that of channels located in the 7.7 µm band due to weaker absorption lines: they won't be considered here. In the 7.7 µm band, channels are sensitive to water vapour (H_2O), nitrous oxide (N_2O) and surface characteristics.

The main interference, as far as CH_4 is concerned, comes from H_2O, which dominates the infrared spectrum in CH_4 absorption bands. Since water vapour variability is quite high, especially in the tropics, and knowledge of its tropospheric distribution still limited, separating the CH_4 signal from water vapour is quite challenging and precludes the use of most of the channels. Due to much lower water vapour content in the mid-latitude regions as opposed to the tropics, the interferences between H_2O

and CH_4 are less pronounced in the extra-tropical regions, causing a higher signal-to-interference ratio over more channels. Altogether, only a few successive channels located in the 7.674- 7.686 µm (1301-1303 cm^{-1}) interval present a low-enough sensitivity to water vapour to be used to retrieve CH_4.

Twenty four channels have been selected to optimize the signal-to-interference ratio. They are not sensitive to variations of CH_4 in two parts of the atmosphere: the lower troposphere (roughly below 500 hPa) and the tropopause (Crevoisier et al., 2003). The Jacobians of the selected channels have very similar shapes and all peak around 260 hPa. Hence, IASI only allows the retrieval of a mid-tropospheric column of CH_4. It is equivalent to say that IASI observations are characterized by only one degree of freedom for CH_4 along the vertical.

3.1.3.2. Channels for CO_2

IASI channels sensitive to carbon dioxide are either located in band v_2 of CO_2, around 15 µm (670 cm^{-1}), or in band v_3, around 4.3 µm (2260 cm^{-1}), and present various sensitivities to other atmospheric or surface components. The 4.3 µm band is characterized by a very high radiometric noise that precludes using this channel for retrieving CO_2. The main interference, as far as CO_2 is concerned, comes from H_2O and ozone. Consequently, use is made of a few successive channels located in the 15 µm band (around 670 cm^{-1}).

As described in section 3.1.7, these channels are not sensitive to variations of CO_2 in two parts of the atmosphere: the lower troposphere (roughly below 500 hPa) and the tropopause (Crevoisier et al., 2003). The Jacobians of the selected channels have very similar shapes and all peak around 200 hPa. Hence, IASI only allows the retrieval of a mid-tropospheric column of carbon dioxide. It is equivalent to say that IASI observations are characterized by only one degree of freedom on the vertical for CO_2.

3.1.4. Neural architecture

The weakness of the signal induced on IASI brightness temperature (BT) by CH_4 or CO_2 variations, associated with the complexity (in particular its non-Gaussianity) of the relationship between the gas concentration and observed BT, makes it difficult to solve this inverse problem. To tackle this problem, use is made of a non-linear inference method, based on the Multilayer Perceptron (MLP) neural network (Rumelhart et al., 1986) with two hidden layers. Following the selection of IASI and AMSU-A channels described previously, the chosen neural architectures are the following.

3.1.4.1. Architecture for CH_4 (version 10.2)

The input layer is composed of:

- 24 IASI BT. Among them, the first 5 channels are not sensitive to CH_4 but to stratospheric temperature only. They have been included in order to deal with the slight sensitivity of the selected CH_4 IASI channels to stratospheric temperature;
- 1 AMSU-A BT of channel 6;
- 5 differences between AMSU-A and IASI BT, given by Table 3, to help the MLP to decorrelate the information from temperature (given by AMSU-A) and CH_4 signal (given by IASI);

Table 3: List of differences between AMSU-A and IASI channels used to retrieve MT-CH_4

AMSU-A channel	6	6	6	6	6
IASI channel	2497	2553	2634	2637	2809

Altogether, there are 30 predictors.

The output layer of the network is composed of:

- the difference between the true value of CH_4 concentration (associated with inputs) and the TIGR reference one (1860 ppb);
- 24 differences between the "true" IASI BT (associated with the true CH_4 concentration value) and the "reference" one (associated with the reference CH_4 concentration value), once again to constrain the solution.

Altogether, there are 25 predictands.

Our past experience and several trials have led us to choose 70 neurons for the first hidden layer and 40 for the second one (Crevoisier et al. 2009a,b).

3.1.4.2. Architecture for CO_2 (version 10.1)

The input layer is composed of:

- 81 IASI BT. Among them, the first 5 channels are not sensitive to CO_2 but to stratospheric temperature only. They have been included in order to deal with the slight sensitivity of the selected CO_2 IASI channels to stratospheric temperature;
- 1 AMSU-A BT of channel 6;
- 8 differences between AMSU-A and IASI BT, given by Table 4, to help the MLP to decorrelate the information from temperature (given by AMSU-A) and CO_2 signal (given by IASI);

Table 4: List of the differences between AMSU-A and IASI channels used to retrieve CO_2

AMSU-A channel	6	6	6	6	6	6	6	6
IASI channel	199	205	207	208	211	214	222	299

Altogether, there are 90 predictors.

The output layer of the network is composed of:

- the difference between the true value of CO_2 concentration (associated with inputs) and the TIGR reference one (395 ppm);
- 81 differences between the "true" IASI BT (associated with the true CO_2 concentration value) and the "reference" one (associated with the reference CO_2 concentration value), once again to constrain the solution.

Altogether, there are 82 predictands.

Our past experience and several trials have led us to choose 90 neurons for the first hidden layer and 50 for the second one (Crevoisier et al. 2009a,b).

3.1.5. Training of the networks

The learning algorithm is the optimization technique that estimates the optimal network parameters by minimizing a positive-definite cost function which measures, for a set of representative situations for which inputs (here the brightness temperatures) and outputs (gas mixing ratios) are known (the learning set), the mismatch between the neural network outputs and the desired outputs. Here, the Error Back-Propagation algorithm (Rumelhart et al., 1986) is used to minimize the following cost function:

$$E = \sum_{i=1}^{N} \int_{qmin}^{qmax} dq[MLP(y_i(q)) - q]^2 \quad (1)$$

where:

- E is the cost function;
- N is the number of atmospheric situations in the training database;
- q is the "true" mixing ratio value;
- $qmin$ and $qmax$ define the range variation of GHG mixing ratio;
- $MLP(y_i(q))$ is the retrieved mixing ratio by the MLP using as inputs the brigtness temperatures of IASI and AMSU-A, noted as $y_i(q)$

It is a gradient descent algorithm well adapted to the MLP hierarchical architecture because the computational cost is linearly related to the number of parameters. To avoid being trapped in local minima during the minimization of the cost function, stochastic steepest descent is used. The learning step is made sample by sample, chosen iteratively and stochastically in the learning data set.

The training database from which the networks learn the relationship existing between inputs and outputs is based on the TIGR database. For all TIGR atmospheric situations, for all scan angles, and for the whole IASI channels used in the retrieval process, clear-sky brightness temperatures, transmittances and Jacobians have been computed using the 4A/OP radiative transfer model with the spectroscopic database GEISA-2011 (Jacquinet-Husson et al. 2011) as input. The required AMSU-A BTs are computed using the STRANSAC microwave forward model (Scott, 1974). Network input BTs correspond to randomly drawn values of concentration in the range 1610-2110 ppb for CH_4 and in the range 345-445 ppm for CO_2, centred on the TIGR reference value of 1860 ppb for CH_4 and 395 ppm for CO_2;. It is worth noting that no prior information is thus given to the networks in terms of seasonality, trend, or geographical patterns of the gases.

Neural networks are trained for each of the 15 AMSU-A scan angles and for 2 air-masses (tropical or mid-latitude) independently. Surface elevation is also taken into account. Altogether, for a given neural architecture, 240 networks are trained. For each network corresponding to one air-mass, one scan angle and one surface type, the learning steps are the following:

1. One atmosphere is randomly chosen among the TIGR atmospheres of the considered air-mass.
2. A GHG mixing ratio is drawn randomly (uniform distribution) in the range 1610-2110 ppb for CH_4 and 345-445 ppm for CO_2, which is centred on the reference GHG mixing ratio of TIGR (1860 ppb for CH_4 and 395 ppm for CO_2). The mixing ratio is assumed to be uniformly constant from the surface to space.
3. A perturbation of the surface temperature is randomly chosen according to the normal distribution, with a null mean value and a standard deviation of 4 K.
4. The input BTs at the drawn GHG mixing ratio are computed using BTs from TIGR for the considered atmosphere.
5. For IASI channels, noise equivalent temperatures are computed at the BT according to:

$$NE\Delta T[T_B(\nu), \nu] = NE\Delta T[T_{ref}, \nu] \frac{\frac{\partial B}{\partial T}(T_{ref}, \nu)}{\frac{\partial B}{\partial T}(T_B(\nu), \nu)} \quad (2)$$

   where $NE\Delta T$ is the equivalent noise temperature taken at the brightness temperature T_B, of the channel located at frequency ν, and B is the radiance. The reference noise corresponding to a reference temperature T_{ref} of 280 K is taken from the in-flight noise measurement (CNES, priv. comm.). To increase the signal to noise ratio, and speed the learning phase, these noises have been divided by 2. Since 4 IASI spots are localized within one AMSU-A spot, the average of IASI BT contained in a single AMSU-A field-of-view are therefore used as inputs to the networks.
6. The instrument noise are is computed and added to the BTs.
7. The inputs and outputs are normalized in order to homogenise the input values between -1 and 1.
8. The Error Back-Propagation algorithm (Rumelhart et al., 1986) is used to minimize the cost function.
9. The parameters of the networks are updated.
10. The networks are applied to the whole ARSA atmospheres following the same procedure as TIGR (steps 4 to 7) and the associated cost function is computed.
11. Go back to step 1, until the predefined number of iterations has been reached.

The ARSA database is used as a test database during training. This allows us to verify that the network is not overfitting. Overfitting means that the network memorizes the training set (here TIGR) so closely that it can no longer make correct predictions on new data (here ARSA). This is observed when the cost function calculated on the ARSA test database increases during training while the cost function on the TIGR training database continues to decrease.

Figure 4 illustrates the learning steps presented before:

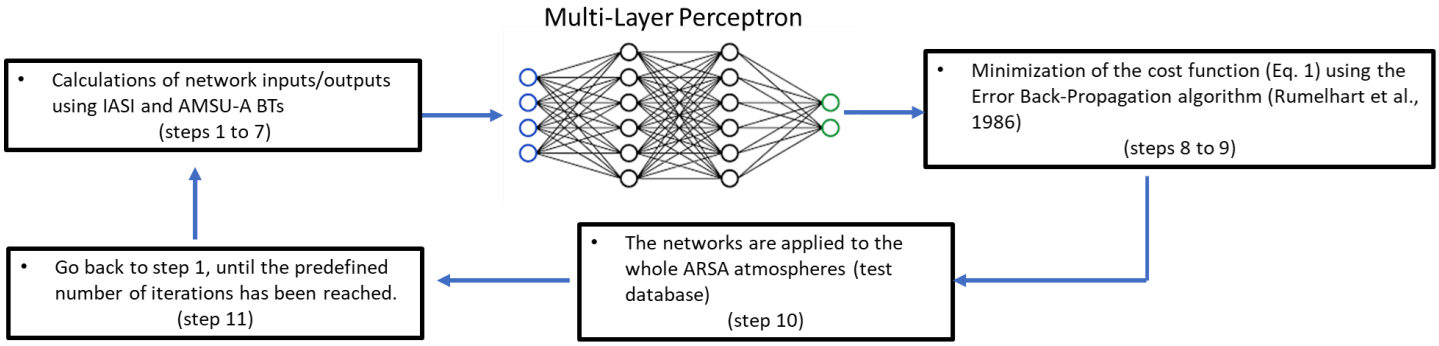

Figure 4: This diagram illustrates the learning steps of one neural network

3.1.6. Application to observations

Once the learning phase is completed, observations of IASI and AMSU-A can be used to infer mid-tropospheric columns of CH_4 or CO_2. The retrieval is performed at the AMSU-A spatial resolution: when 4 IASI FOVs included in 1 AMSU-A FOV are declared clear (meaning that no cloud or aerosol has been detected), the BTs of the channels are averaged over the 4 IASI FOVs and used together with AMSU-A BTs, to perform the retrieval.

Since the networks are trained with simulated data, potential systematic radiative biases existing between simulations used in the learning phase and observations must be removed before using these BTs as inputs to the network corresponding to the situation based on the scan angle, surface elevation and air-mass type. These systematic radiative biases are computed with the calibration/validation chain that has been developed for many years at LMD (Armante et al., 2016). For each channel, the differences between simulations and collocated (in time and space) satellite observations are averaged over several full years of operation. These differences are called 'calc-obs' residuals. The simulations are performed using the 4A/OP forward model and radiosonde measurements from ARSA as inputs. One key element is that, during

this computation, the CH_4 and CO_2 mixing ratios are kept at the reference value of the TIGR database (1860 ppb and 395 ppm respectively) to avoid making the CH_4 or CO_2 signals disappearing in the BT used as input to the networks. Every month, about 100 collocations are available, giving access to robust statistics.

By averaging thousands of situations together, it is possible to derive the change in the averaged biases with the scan angle. In order to avoid potential biases due to the incorrect modelling of the radiative effect of hight viewing scan angles close to the edges of the orbit, which is particularly the case for microwave observation, specific radiative biases have to be taken into account for each scan angle.

3.1.7. Vertical characterization of the retrieval

As stated before, IASI channels located in the 7.7 µm and 15 µm bands are mostly sensitive to tropospheric variations of gases. The averaging kernels, which indicate which part of the atmosphere the retrievals are representative of, are determined through radiative transfer simulations. A uniform perturbation of CH_4 or CO_2 mixing ratio is applied sequentially to each of the 40 pressure layers used in ARSA to characterize atmospheric profiles. IASI and AMSU-A brightness temperatures are then computed by the 4A/OP model for each of the perturbed atmospheric profiles and used as inputs to the neural networks. The theoretical change F_i in ppbv/ppbv for MT-CH_4 and ppm/ppm for MT-CO_2 of the column mean apparent mixing ratio ($\widehat{q}$) given a mixing ratio perturbation of dq^{ref} applied to the mixing ratio q_i at level *i*, is then given by:

$$F_i = \frac{\widehat{q}(q_i + dq^{ref}) - \widehat{q}(q_i)}{dq^{ref}} \quad (3)$$

The mean of the averaging kernel for CH_4 computed over the ARSA dataset is plotted in Figure 5. In the tropics, the height of the tropopause is approximately 17 km, whereas it is closer to 8 km in the mid-latitudes. The non-linear inference scheme gives access to a mid-to-upper tropospheric integrated content of CH_4 covering: (i) the range 100-500 hPa (roughly 9-15 km), with the highest sensitivity around 230 hPa in the tropics; (ii) the range 250-700 hPa (roughly 6-12 km), with the highest sensitivity around 400 hPa in the mid-latitudes.

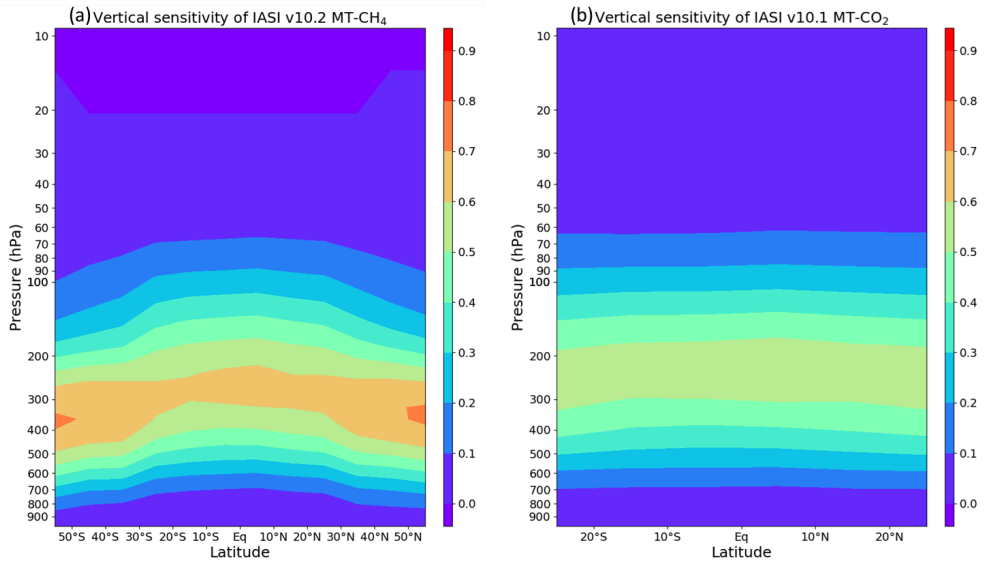

Figure 5: Vertical sensitivity of IASI v10.2 MT-CH_4 retrievals (a) and v10.1 MT-CO_2 retrievals (b) as a function of latitude.

3.2. Algorithm for L3 MTCO2_OBS4MIPS and MTCH4_OBS4MIPS products

To generate L3 MTCO2_OBS4MPIS and MTCH4_OBS4MPIS products, MT-CO_2 and MT-CH_4 averages (one for each product) are computed within each 1°X1° grid box and per day and using all L2 MT-CO_2 and MT-CH_4 available.

For that:

1. L2 MT-GHG (MT-CO_2 or MT-CH_4) retrievals available for the same day and for each 1°X1° grid box have been regrouped;
2. For each 1°X1° grid box, MT-GHG averages are computed as the median to ensure that these averages are not impacted by possible outliers. The associated averaging kernel corresponds to the MT-GHG closest to the median.

The availability of L2 MT-CO_2 and MT-CH_4 products for the three Metop-A, -B and -C platforms between July 2007 and December 2023 is illustrated in Figure 3.

4. Output data

The output data products are mid-tropospheric column mixing ratios (mole fractions) of CO_2 and CH_4, denoted as MT-CO_2 and MT-CH_4 plus related quantities.

Table 5 provides an overview of the L3 MT-CO_2 and MT-CH_4 data products. The product format is described in the MTGHG PUGS, 2024.

Table 5: Overview of MT-CO_2 and MT-CH_4 Obs4MIPs data products. These data are generated in Obs4MIPs format (Observations for Model Intercomparisons Project, described in the MTGHG PUGS, 2024).

Product ID	Level	Sensor(s)	Comments
MTCO2_OBS4MIPS	3	Merged: Metop-A Metop-B Metop-C	Temporal resolution: daily Spatial resolution: 1^ox1^o Latitude range: Tropics (about 30°S:30°N)
MTCH4_OBS4MIPS	3	Merged: Metop-A Metop-B	Temporal resolution: daily

		Metop-C	Spatial resolution: 1°x1° Latitude range: Tropics and mid-latitudes (about 60°S:60°N)

These L3 products have been generated in Obs4MIPs format.

The MTCO2_OBS4MIPS and MTCH4_OBS4MIPS products consist of daily, 1°x1° gridded L3 MT-CO_2 or MT-CH_4 from the three Metop platforms. These product files contain the geolocation information (latitude, longitude and time), the MT-CO_2 and MT-CH_4 medians, the associated standard deviations of the L2 MT-CO_2 and MT-CH_4, the number of products used to calculate the averages and the averaging kernels.

For details on the product format and the validation, see MTGHG PUGS and MTGHG PQAR, 2024.

The MTCO2_OBS4MIPS and MTCH4_OBS4MIPS products are available using the following links:

- Direct link to CO_2 products: https://cds.climate.copernicus.eu/datasets/satellite-carbon-dioxide?tab=overview, DOI: 10.24381/cds.f74805c8
- Direct link to CH_4 products: https://cds.climate.copernicus.eu/datasets/satellite-methane?tab=overview, DOI: 10.24381/cds.b25419f8

For example, Figure 6 and Figure 7 show respectively for August 2020 monthly average maps of L3 MT-CO_2 (Figure 6 (a)) and L3 MT-CH_4 (Figure 6 (b)) and the associated standard deviations of L3 MT-CO_2 (Figure 7 (a)) and L3 MT-CH_4 (Figure 7 (b)). To obtain these figures, the daily MT-CO_2 and MT-CH_4 Obs4MIPs data were averaged over the month of August 2020 for each 1°X1° grid.

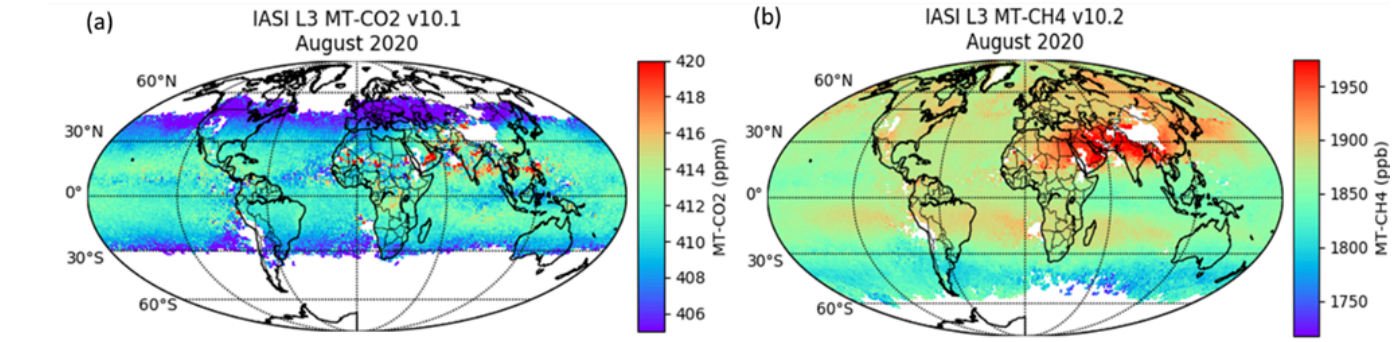

Figure 6: Examples of maps of MTCO2_OBS4MIPS (a) and MTCH4_OBS4MIPS (b) for August 2020

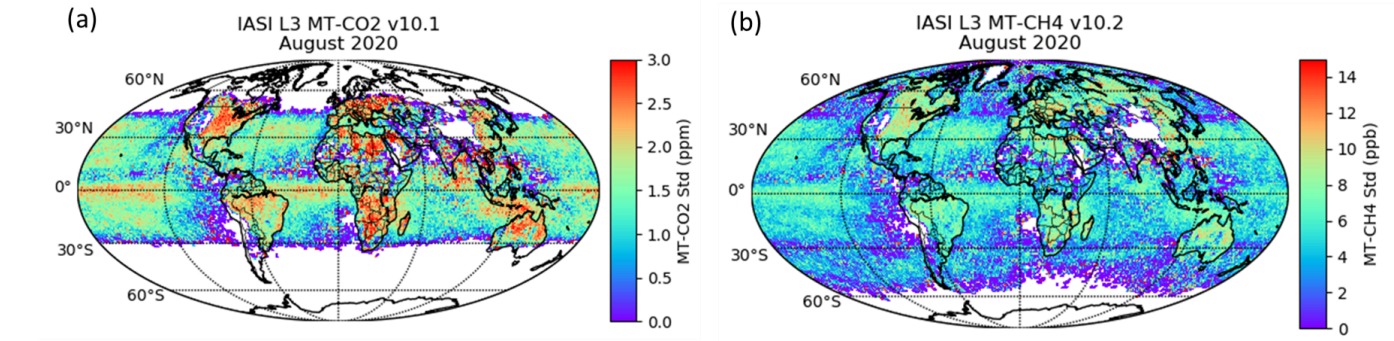

Figure 7: Examples of maps of MTCO2_OBS4MIPS (a) and MTCH4_OBS4MIPS (b) standard deviations for August 2020

Acknowledgments

We acknowledge previous funding by the European Space Agency (ESA) via Climate Change Initiative (CCI) project GHG-CCI. This funding enhanced the quality of the retrieval algorithms and related documentation. This resulted in more mature data products as needed for an operational project such as the Copernicus Climate Change Service (C3S). We also acknowledge the ESPRI computing center.
The development of retrieval algorithms based on IASI observations would have not been possible without the strong support of CNES.
We thank the AirCore-Fr team for providing AirCore data and CONTRAIL team for providing aircraft measurements of greenhouse gases.

References

Armante et al., 2016: Armante, R., Scott, N., Crevoisier, C., Capelle, V., Crepeau, L., Jacquinet, N., Chédin, A., Evaluation of spectroscopic databases through radiative transfer simulations compared to observations. Application to the validation of GEISA 2015 with IASI and TCCON, Journal of Molecular Spectroscopy, Volume 327, 2016, Pages 180-192, ISSN 0022-2852, 2016, https://doi.org/10.1016/j.jms.2016.04.004

Bojinski et al., 2014: Bojinski, S., M. Verstraete, T.C. Peterson, C. Richter, A. Simmons, M. Zemp, The Concept of Essential Climate Variables in Support of Climate Research, Applications, and Policy. Bull. Amer. Meteor. Soc., 95, 1431–1443. Available at http://journals.ametsoc.org/doi/pdf/10.1175/BAMS-D-13-00047.1, 2014.

CMUG-RBD, 2012: Climate Modelling User Group Requirements Baseline Document, Deliverable 1.2, Number D1.2, ESA Climate Change Initiative (CCI), Version 2.0, 17 Dec 2012, 2012. Link: https://climate.esa.int/media/documents/CMUG_D1.2_URD_v2.0.pdf

Chédin et al., 2003: Chédin, A., Saunders, R., Hollingsworth, A., Scott, N. A., Matricardi, M., Etcheto, J., Clerbaux, C., Armante, R. and Crevoisier, C.: The feasibility of monitoring CO_2 from high resolution infrared sounders. J. Geophys. Res., 108, ACH 6-1–6-19, doi: 10.1029/2001JD001443, 2003. https://doi.org/10.1029/2001JD001443

Chevallier el al., 1998: Chevallier, F., F. Chéruy, N. A. Scott, and A. Chédin, 1998: A Neural Network Approach for a Fast and Accurate Computation of a Longwave Radiative Budget. *J. Appl. Meteor. Climatol.*, 37, 1385–1397, https://doi.org/10.1175/1520-0450(1998)037<1385:ANNAFA>2.0.CO;2.

Crevoisier et al., 2003: Crevoisier, C., Chedin, A. and Scott, N.A., AIRS channel selection for CO2 and other trace-gas retrievals 129, 2719–2740. doi:10.1256/qj.02.180, 2003. https://doi.org/10.1256/qj.02.180

Crevoisier et al., 2009a: Crevoisier, C., Chédin, A., Matsueda, H., et al., First year of upper tropospheric integrated content of CO_2 from IASI hyperspectral infrared observations, *Atmos. Chem. Phys.*, 9, 4797-4810, https://doi.org/10.5194/acp-9-4797-2009, 2009.

Crevoisier et al., 2009b: Crevoisier, C., Nobileau, D., Fiore, A., Armante, R., Chédin, A., and Scott, N. A.: Tropospheric methane in the tropics – first year from IASI hyperspectral infrared observations, Atmos. Chem. Phys., 9, 6337–6350, doi:10.5194/acp-9-6337-2009, https://doi.org/10.5194/acp-9-6337-2009, 2009.

Crevoisier et al., 2013: Crevoisier, C., Nobileau, D., Armante, R., et al., The 2007–2011 evolution of tropical methane in the mid-troposphere as seen from space by MetOp-A/IASI, *Atmos. Chem. Phys.*, 13, 4279-4289, https://doi.org/10.5194/acp-13-4279-2013, 2013.

Jacquinet-Husson et al. 2011: Jacquinet-Husson N., L. Crépeau, R. Armante, C. Boutammine, A. Chédin, et al.. The 2009 edition of the GEISA spectroscopic database, J. Quant. Spectrosc. Radiat. Transfer,112, 2395-2445 doi:10.1016/j.jqsrt.2011.06.004, https://doi.org/10.1016/j.jqsrt.2011.06.004, 2011.

Machida et al. 2008: Machida, T., Matsueda, H., Sawa, Y., Nakagawa, Y., Hirotani, K., Kondo, N., Goto, K., Nakazawa, T., Ishikawa, K., and Ogawa, T.: Worldwide measurements of atmospheric CO_2 and other trace gas species using commercial airlines, J. Atmos. Ocean. Tech., 25(10), 1744–1754, doi:10.1175/2008JTECHA1082.1, 2008, https://doi.org/10.1175/2008JTECHA1082.1

Membrive et al. 2017: Membrive, O., Crevoisier, C., Sweeney, C., Danis, F., Hertzog, A., Engel, A., Bönisch, H., and Picon, L.: AirCore-HR: a high-resolution column sampling to enhance the vertical description of CH_4 and CO_2, Atmos. Meas. Tech., 10, 2163-2181, https://doi.org/10.5194/amt-10-2163-2017, 2017.

National Research Council, 2004: National Research Council, Climate Data Records from Environmental Satellites: Interim Report 2004, 150 pp., ISBN: 978-0-309-09168-8, DOI: https://doi.org/10.17226/10944, 2004.

Parkinson et al., 2006: Parkinson, C., A. Ward and M. King, Earth Science Reference Handbook, NASA, Washington DC, 2006.

PQAR MTGHG, 2024: Crevoisier, C., Meilhac, N., C3S Greenhouse Gas (GHG: MTCO2 v10.1 & MTCH4 v10.2): Product Quality Assessment Report (PQAR)

PUGS MTGHG, 2024: Crevoisier, C., Meilhac, N., C3S Greenhouse Gas (GHG: MTCO2 v10.1 & MTCH4 v10.2): Product User Guide and Specification (PUGS)

Rumelhart et al., 1986: Rumelhart, D.E. and McClelland, J.L. (1986) University of California, S.D.P.R.G. Parallel distributed processing : explorations in the microstructure of cognition, Parallel distributed processing: explorations in the microstructure of cognition, vol. 1. MIT Press. https://doi.org/10.7551/mitpress/5236.001.0001

Scott, 1974: Scott, N.A., A direct method of computation of the transmission function of an inhomogeneous gaseous medium— I: Description of the method. J. Quant. Spectrosc. Radiat. Transf. 14, 691–704. https://doi.org/10.1016/0022-4073(74)90116-2

Scott and Chédin, 1981: Scott, N.A. and Chédin, A., A Fast Line-by-Line Method for Atmospheric Absorption Computations: The Automatized Atmospheric Absorption Atlas. J. Appl. Meteorol. 20, 802–812. https://doi.org/10.1175/1520-0450(1981)020%3C0802:AFLBLM%3E2.0.CO;2

TRD GAD GHG, 2024: Buchwitz, M., et al., Target Requirement and Gap Analysis Document, Copernicus Climate Change Service (C3S) project on satellite-derived Essential Climate Variable (ECV) Greenhouse Gases (CO_2 and CH_4) data products (project C3S2_312a_Lot2), Version 5.6, 22-Mar-2024, pp. 87, 2024. Latest version: http://wdc.dlr.de/C3S_312b_Lot2/Documentation/GHG/C3S2_312a_Lot2_TRD-GAD_GHG_latest.pdf

Werschek, 2015: Werschek, M., EUMETSAT Satellite Application Facility on Climate Monitoring, C3S Climate Data Store workshop, Reading, UK, 3-6 March 2015. https://www.ecmwf.int/sites/default/files/elibrary/2015/13546-existing-solutions-eumetsat-satellite-application-facility-climate-monitoring.pdf

Wofsy et al. 2012: Wofsy, S. C., Daube, B. C., Jimenez, R., et al.: HIPPO Merged 10-second Meteorology, Atmospheric Chemistry, Aerosol Data (R 20121129), Carbon Dioxide Information Analysis Center, Oak Ridge National Laboratory, Oak Ridge, Tennessee, USA, https://doi.org/10.3334/CDIAC/HIPPO_010 (Release 29 November 2012), 2012.

Related articles

C3S Greenhouse Gas (GHG: MTCO2 v10.1 & MTCH4 v10.2): Product Quality Assessment Report (PQAR) (Copernicus Knowledge Base)
ecv c3s-ghg c3s-ch4 c3s-co2

C3S Greenhouse Gas (GHG: MTCO2 v10.1 & MTCH4 v10.2): Algorithm Theoretical Basis Document (ATBD) (Copernicus Knowledge Base)
ecv c3s-ghg c3s-ch4 c3s-co2

C3S Greenhouse Gas (GHG: MTCO2 v10.1 & MTCH4 v10.2): Product User Guide and Specification (PUGS) (Copernicus Knowledge Base)
ecv c3s-ch4 c3s-co2 c3s-ghg

ecv c3s-ghg c3s-ch4 c3s-co2

Feedback: C3S User Satisfaction Survey - CAMS User Satisfaction Survey

Web: C3S Help and Support - CAMS Help and Support

PROGRAMME OF THE EUROPEAN UNION

Copernicus Europe's eyes on Earth

IMPLEMENTED BY ECMWF